

Morphological, Structural and Optical Properties of Ba-Doped NiO Nanostructure Thin Films

M.Z. Merad¹, L. Fellah^{2,*}, A. Diha³

¹ *Exploitation et Valorisation des Ressources Naturelles en Zones Arides, 30000 Ouargla, Algeria*

² *Faculty of Hydrocarbons and Renewable Energies and Earth and Universe Sciences, University of Kasdi Merbah, 30000 Ouargla, Algeria*

³ *Department of Mechanical Engineering, University Larbi Tébessi, Tébessa 12000, Algeria*

(Received 21 August 2023; revised manuscript received 14 October 2023; published online 30 October 2023)

This paper reports the effect of barium doping on NiO thin films. Undoped and doped films thin films were deposited on a glass substrate at 450 °C using pneumatic spray pyrolysis technique (PSPT) with different concentrations of barium (0 – 8 at. %). X-ray diffraction patterns show the polycrystalline nature of the films with the preferred orientation (111). No other barium metal cluster and impurity phases have been observed with Ba doping. The crystal size of the deposited thin films was calculated using the Debye-Scherrer formula for the two orientations (111) and (200), and from the SEM photographs, we found values ranging from 11.95 to 39.06 nm in both cases. In the visible region, the optical transmission of Ba-doped NiO thin films dropped by up to 46 % when compared to undoped NiO thin films (79 %). The band gap was found to be decreasing in the range of 3.742 – 3.503 eV with Ba doping. The Urbach disorder energy clearly increases from 262.98 to 356.64 meV when passing from the undoped thin layer to the thin layer doped at 2 at. %, then decreases to the minimum 303.14 meV for a barium doping of 8 at. %, allowing the atoms to find a good site, i.e. thin films become homogeneous and highly crystallized. The roughness was calculated using SEM image analysis. Its values were ranged between 23.26 – 39.06 nm.

Keywords: Spray pyrolysis, Ba doped NiO, Thin films, Band gap, Urbach energy, Grain size.

DOI: [10.21272/jnep.15\(5\).05013](https://doi.org/10.21272/jnep.15(5).05013)

PACS numbers: 61.43.Dg, 68.55. Ln, 68.55.jd

1. INTRODUCTION

Transparent conducting oxides (TCO's) are essential in many areas of chemistry, physics, and materials science because they have numerous potential uses such as capacitors for electrochemical reactions, photovoltaic cells, gas sensors, and so on.

Karl Baedeker, who discovered that a thin film of cadmium oxide (CdO) is both transparent and conductive in 1907, inspired interest in TCO's [1]. As result, much emphasis has been devoted on the growth and synthesis of nanostructured metal oxide materials such as SnO₂, ZnO, InO₃, CuO, MoO₃, and CdO. However, the significant advances in the realm of TCO's occurred with J. T. Littleton's discovery of tin oxide (SnO₂) in 1931 [2], and the doping of this oxide with antimony (SnO₂: Sb) [3], chlorine (SnO₂: Cl) [4] and fluorine (SnO₂: F) [5] in 1946, 1947, and 1951, respectively. Further research concentrated on the creation of indium oxide (In₂O₃) [6] in the 1940s and 1950s. J.M. Mochel discovered tin-doped indium oxide (In₂O₃: Sn) [7], often known as ITO (Indium Tin Oxide), in 1951. E. Scharowsky investigated the optical and electrical characteristics of zinc oxide (ZnO) in 1953 [8]. The following decades saw the research and development of indium and zinc-based OTCs, culminating in the first time in 1971[9] with the invention of aluminum-doped zinc oxide (ZnO: Al or AZO) with characteristics similar to ITO. It should be mentioned that gallium-doped zinc oxide (ZnO: Ga or GZO), which was made later, performed admirably as well. In the 1990s, complex TCO's were developed by combining multiple components (In, Zn, Cd, Sn, and Ga).

NiO is one of these TCO materials known for its

unique physical and chemical stability, and has been the subject of many recent studies [10]. In general, pure stoichiometric NiO is an insulator but, when prepared as thin films, it is a metal-deficient p-type semiconductor with a bandgap width in the range 3.5 – 4.0 eV [11,12].

The goal of this research is to synthesize thin layers of Ba-doped NiO and investigate the effect of Ba doping on the microstructural and optical properties of these layers. Unlike other elements, barium doping has been widely used in the fields of glasses and ceramics, but not substantially enough in thin films.

2. EXPERIMENTAL PROCEDURE

2.1 Preparation of Simples

NiO: Ba thin films (0 – 8 at. %) were deposited on corning glass substrates. Spray-pyrolysis is the deposition technique employed. In this procedure, we prepared two solutions: a solution of the main precursor based on Nickel chloride and a second solution based on barium chloride containing the doping element Ba. Nickel chloride hexa hydrate [NiCl₂.6H₂O] was dissolved in a 1:4 mixture of ethanol and distilled water to make a 0.15 M solution of undoped NiO. The solution was stirred for about 1.5 hours at a constant temperature of 90 °C. while the volume of the solution kept constant. The same procedure was used to prepare a dopant solution of 0.5 M BaCl₂. An appropriate quantity of barium hexa hydrate chloride [BaCl₂.6H₂O] was dissolved in 100 mL of distilled water mixed with ethanol. In every case, the deposited solution is formed by a mixture of two well-defined volumes derived from previous solutions. The corning glass substrates were ultrasonically cleaned three times

* fellahcene@yahoo.fr

in succession with three distinct mixtures: distilled water and HCl, acetone and distilled water, and distilled water. The thin films were deposited by sprayed onto heated substrates at 450 °C using a heating plate. The solution was sprayed at a pressure of 1.5 bars and a distance of 25 cm (nozzle-substrate). We deposited 15 mL of the doped solution to prepare each sample. The pulverization time was 10 s separated by 40 s to keep the substrate temperature constant. The reference sample was undoped NiO. The Ba content varied as 2, 4, 6 and 8 at. %.

2.2 Devices and measurements

The micro-crystalline structure of deposited NiO thin films was determined through X-ray diffraction (XRD) on a Bruker (D8 ADVANCE) Diffractometer. The X-ray source was a copper cathode with $\lambda(\text{Cu-K}\alpha) = 1.54056 \text{ \AA}$. The surface morphology was studied by scanning electron microscope (SEM) using Quanta-FEG system. The optical transmittance spectra were obtained using UV-visible spectrophotometer (Varian Cary 50 Scan UV Visible Spectrophotometer), and taking into account the glass in the reference beam.

3. RESULTS AND DISCUSSION

3.1 Structural Properties

Fig. 1 shows the XRD spectra of NiO: Ba thin films prepared on corning glass substrates in the 2θ range of 30 – 85°. The diffraction peaks were indexed by comparing the data with ICDD card No. 04-047-1049. The films were observed to be polycrystalline in nature, with a preferential orientation of (111). The four major peaks at 37.09°, 42.86°, 61.13°, and 74.08° correspond to the (111), (200), (220), and (311) orientations of NiO, respectively. These peaks have different intensities and belong to the face-centered cubic NiO phase.

It is important to note that the maximum intensity of the diffraction peaks of Ba-doped NiO films decrease with increasing Ba concentration. This is contrary to what was observed by S. Boulila et al. [12], where the intensity of the peaks seemed to decrease as the barium content increased and as their position shifted towards larger angles.

These changes in intensity and peak position may arise from the size of the Ba atom, which is larger than that of Ni (covalent radius ratio: $r(\text{Ba}^{+2})/r(\text{Ni}^{+2}) = 1.942$). Lattice distortion resulting from the insertion of heavy and larger Ba atoms induces defects in the crystal lattice. The mismatch between the ionic radii of atoms Ba ($r(\text{Ba}^{2+}) = 0.135 \text{ nm}$) and Ni ($r(\text{Ni}^{2+}) = 0.069 \text{ nm}$) creates a lattice distortion, which leads to dislocations and vacancies.

The full width at half maximum (FWHM) of the (111) and (002) peaks of all samples was obtained using the Gaussian fitting tool. The microstructural parameters were calculated from these two diffraction peaks.

The grain size (D) was calculated by the Debye-Scherrer equation [11]:

$$D = \frac{K \cdot \lambda}{\beta_{FWHM} \cdot \cos \theta}, \quad (1)$$

Where $K = 0.98$ which corresponds to spherical shape of grains, λ is the X-ray wavelength of Cu-K α (1.54056 Å), θ is the diffraction angle (in radians) and β_{FWHM} is the full width at half maximum of the peak.

The values of dislocation densities (δ) are calculated using the following relation [11]:

$$\delta = \frac{1}{D^2}, \quad (2)$$

Where D is the grain size.

According to cubic symmetry and considering the first order of diffraction ($n = 1$), the lattice constant can be computed from Eq. (3) and Eq.(4) [13]:

$$2d_{hkl} \cdot \sin \theta = n\lambda, \quad (3)$$

$$d_{hkl} = \frac{a_{hkl}}{\sqrt{h^2 + k^2 + l^2}}, \quad (4)$$

Where h , k , and l are the Miller indices, n is X-ray diffraction order, θ is the Bragg angle, d_{hkl} is the interplanar spacing and λ is the wavelength of used X-ray.

The lattice strain (ε) is calculated using the following relation [14]:

$$\varepsilon = \frac{\beta_{FWHM} \cdot \cos \theta}{4}, \quad (5)$$

The variations in the angles of the diffraction peaks corresponding to the (111) and (200) planes, as well as the size of the crystallites, are shown in Figures (2a) and (2b). These variations illustrate the influence of the barium doping rate on the characteristics of the diffraction peaks and on the crystallites forming the thin layers of NiO.

As the barium concentration increases, the diffraction peaks corresponding to the (111) and (200) planes shift towards larger angles, reaching a maximum value for 8 at. % of Ba dopant.

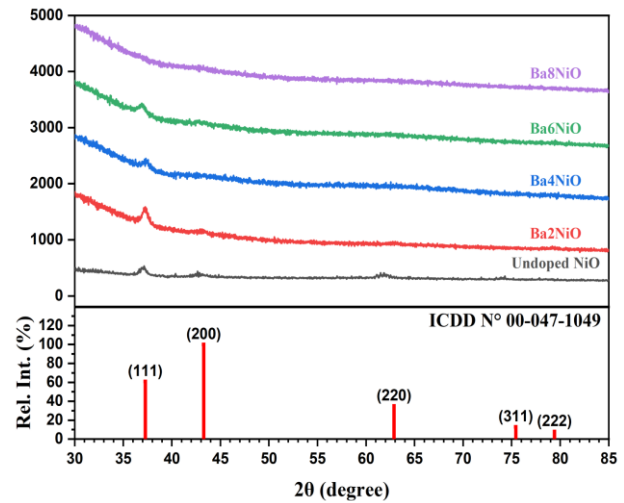


Fig. 1 – X-ray diffraction spectra of undoped NiO and Ba doped NiO thin films prepared at 450 °C, with different concentration of barium

However, for 6 at. % of Ba, these peaks move in the opposite direction. The size of the crystallites, calculated from these same crystalline planes, follows a similar pattern of variation to that of the positions of the diffraction peaks. The maximum crystallite size values were reached for a concentration of 8 at. % of Ba (Tables 1 and 2).

The increase in crystallite size indicates a significant improvement in the crystallinity of the deposited

thin films of Ba-doped NiO, accompanied by an axial orientation that promotes film growth. These phenomena have been observed in previous studies.

It has been reported that this result can be attributed to crystallite coalescence within the thin films and enhanced oxygen diffusion activated by the high temperature used in this experiment (in this work, the temperature was set at 450 °C).

Table 1 – The structural parameters of Ba doped NiO thin films as function of Ba doping percentage of (111) diffraction peak

Samples	2θ	$\beta(FWHM)$	d	α	D	δ	ε
	(°)	(rad)	(nm)	(nm)	(nm)	(Lines/nm ²)	(%)
Undoped NiO	37.090	0.01224	0.24220	0.41949	11.95	7.00E-03	0.506
NiO: Ba 2 at. %	37.340	0.00871	0.24063	0.41678	16.80	3.54E-03	0.360
NiO: Ba 4 at. %	37.418	0.00762	0.24015	0.41595	19.20	2.71E-03	0.315
NiO: Ba 6 at. %	36.851	0.01525	0.24371	0.42212	9.59	1.09E-02	0.631
NiO: Ba 8 at. %	37.353	0.00443	0.24055	0.41665	33.02	9.17E-04	0.183

Table 2 – The structural parameters of Ba doped NiO thin films as function of Ba doping percentage of (200) diffraction peak

Samples	2θ	$\beta(FWHM)$	d	α	D	δ	ε
	(°)	(rad)	(nm)	(nm)	(nm)	(Lines/nm ²)	(%)
Undoped NiO	42.860	0.01003	0.21083	0.42166	14.85	4.54E-03	0.407
NiO: Ba 2 at. %	43.367	0.01089	0.20848	0.41697	13.70	5.33E-03	0.442
NiO: Ba 4 at. %	43.434	0.00762	0.20818	0.41635	19.58	2.61E-03	0.309
NiO: Ba 6 at. %	42.704	0.01743	0.21157	0.42313	8.54	1.37E-02	0.708
NiO: Ba 8 at. %	43.522	0.00279	0.20778	0.41555	53.53	3.49E-04	0.113

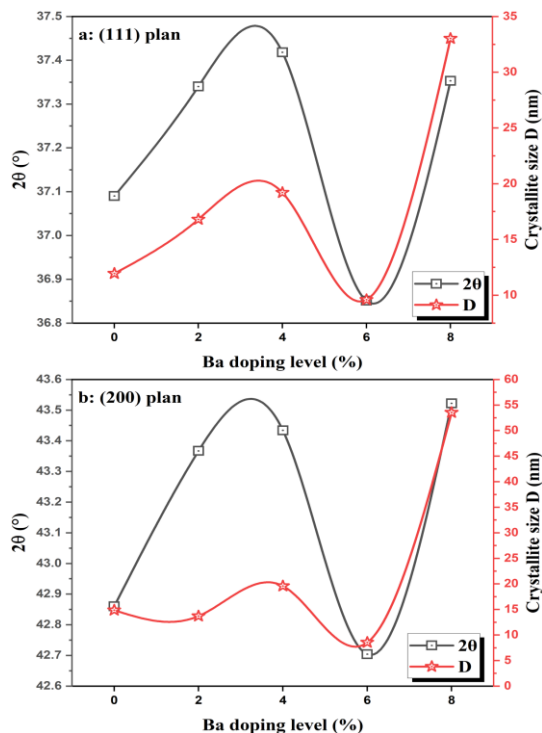


Fig. 2 – The variation of crystallite size and diffraction angle of Ba doped NiO thin films according to a) (111) plan and b) (200) plan

3.2 Morphological Characteristics

Fig. 3a-e show the morphology of as-deposited NiO thin films with various Ba doping concentrations. The scanning electron microscopy (SEM) images show well-defined nanostructures and a close morphological similarity among the as-deposited NiO nanoparticles. These

nanoparticles have regular shapes that include spherical and elliptical morphologies. The clustering of nanoparticles occurred in the majority of cases.

Multiple parameters, including the temperature of the substrate and the concentration of the precursor solution [15], have been reported to affect the size and shape of nanoparticles. SEM analysis provided further information on sample size and shape.

Table 3 summarizes the statistical outcomes acquired from these images. The results correlate well with the particle size estimated by XRD using the Debye-Scherrer formula [Eq. (1)].

Fig. 3a shows the appearance of cracks in the thin film. This is caused by a number of cracking phenomena assumptions, such as cracks between large grains emerging as small grains became closer and agglomerated at the heating temperature and shrinking during cooling, as well as stress and strain produced through coalescence processes.

It should be pointed out that the surface of the films is rough under the experimental conditions used, as illustrated in Fig. 4. The roughness was calculated by SEM image analysis [16]. The measured values fell within a range of (23.26 – 39.06 nm).

Table 3 – Statistical outcomes acquired from SEM images.

Samples	Grain size: D (nm)			
	Mean	Min.	Max.	SD
Undoped NiO	12.50	7.30	19.60	2.78
Ba2 at. %NiO	22.30	17.10	29.40	2.75
Ba4 at. %NiO	23.29	11.70	35.10	4.56
Ba6 at. %NiO	20.75	7.70	38.10	6.65
Ba8 at. %NiO	27.11	10.40	60.00	9.75

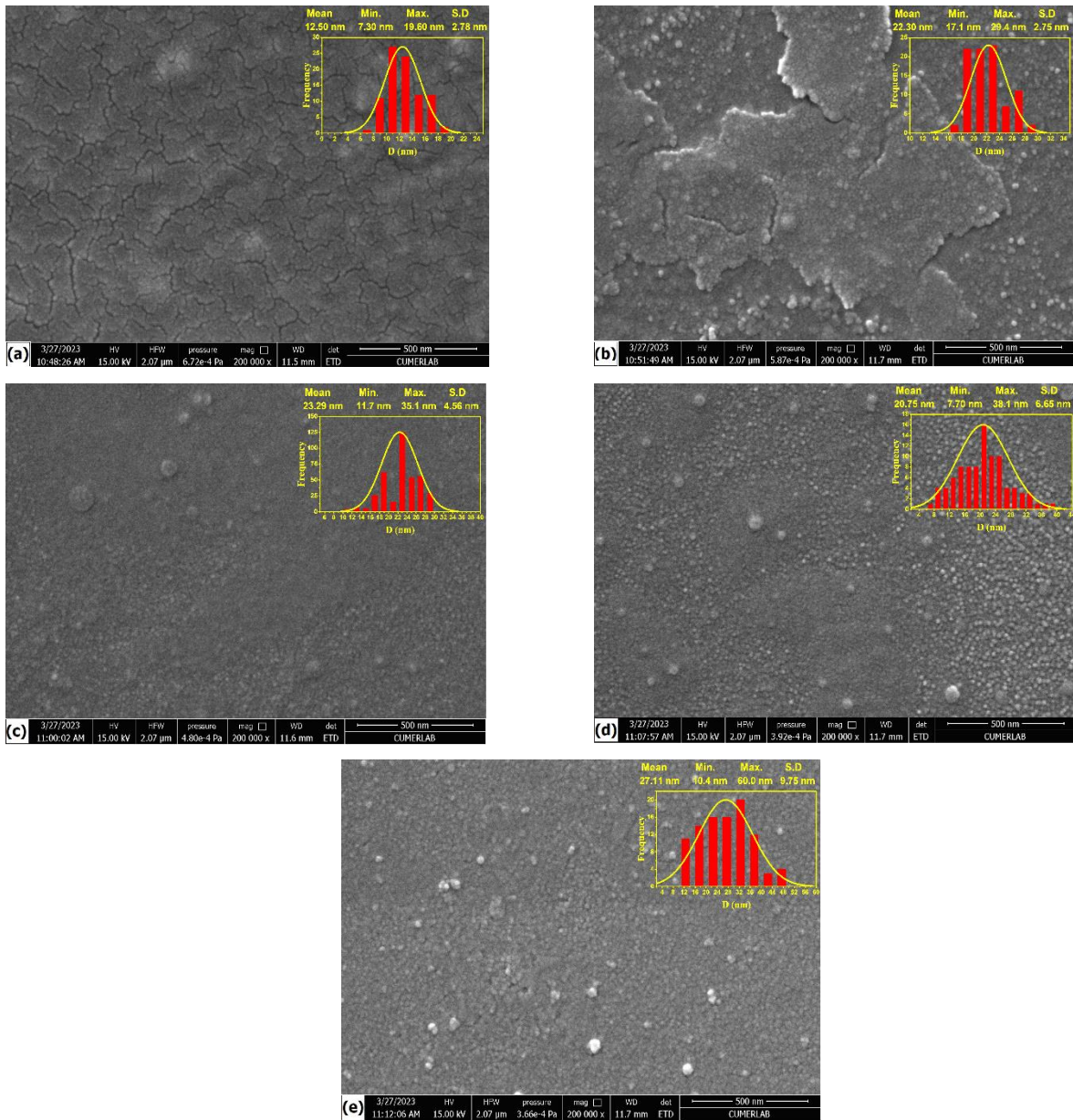


Fig. 3 – SEM images of thin films of NiO as deposited: (a) undoped NiO, (b) Ba 2 at. % NiO, (c) Ba 4 at. % NiO, (d) Ba 6 at. % NiO and (e) Ba 8 at. % NiO. At the top right of each image, the corresponding static histogram has been inserted

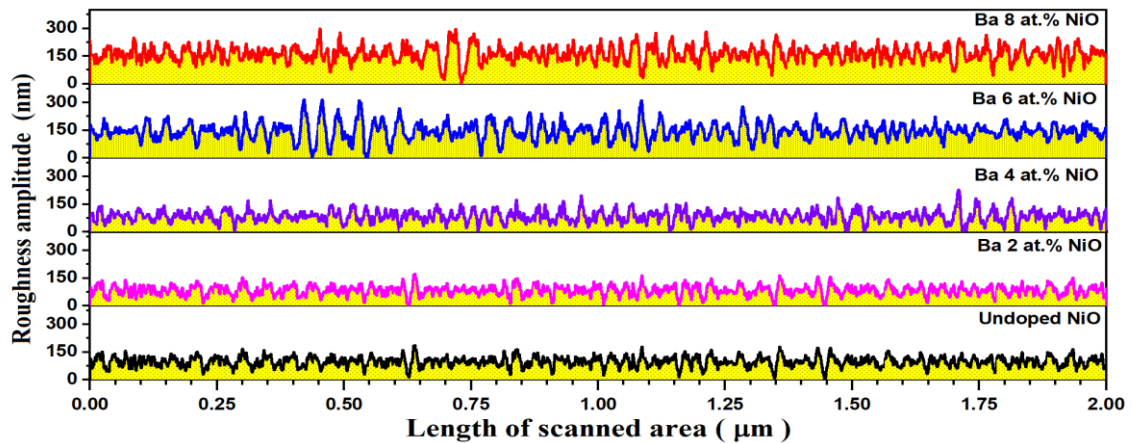


Fig. 4 – Plots of roughness amplitude of undoped NiO and Ba doped NiO thin films deposited at 450 °C

3.3 Optical Properties

The transmission spectra of sprayed thin films of undoped NiO and Ba-doped NiO in the wavelength range 300 – 800 nm are shown in Fig. 3. Transmission is found to be approximately 70 % for an undoped sample and decreases with increasing doping concentration. This is due to a decrease in the grain size (Table 1 and 2), which leads to a rise in grain boundary density. This phenomenon is explained by the difference in atomic radius between Ba and Ni, which causes reduction in transmission.

The absorption coefficient (α) was used to determine the optical band gap of the films using the following relation [17]:

$$\alpha hv = C(hv - E_g)^m, \quad (6)$$

Where C is a constant, E_g is the band gap energy between the valence band and the conduction band, and m index value for direct transition is 1/2.

As illustrated in Fig. 6a-e, the optical band gaps of all samples are measured by plotting the quantity $(\alpha hv)^2$ versus the photon energy (hv). The E_g values of the films were determined for each sample by expanding the linear part of the plot to $(\alpha hv)^2 = 0$. The results are summarized in Table 4.

As seen in Table 4, there is irregular variance in the E_g values with varied barium percentage values. The variation in energy band gap values for crystalline films can be explained [18,19]: (1) a stress-induced band distortion caused by the film/substrate interaction, (2) line and planar defects in the crystalline film, and (3) crystalline size, which affects band bending at particle boundaries. In this case, crystalline defects caused by barium concentration may have a significant impact on the E_g results.

The calculated band gap energies of undoped NiO and Ba doped NiO thin films are in the range of (3.503 – 3.742 eV), which is close to the value (3.71 eV) published by Guziejewicz et al. [20] for nanocrystalline NiO films generated by magnetron sputtering in pure argon. Furthermore, the values reported regarding our nanostructure film (3.503 – 742 eV) are less than that found for the bulk material (4.0 eV) [21]. The quantum confinement effects are well known to cause a blue shift in the spectra of nanoscale semiconductors. However, the obtained values of E_g were less than what was found in the bulk sample. This effect is most likely induced by chemical defects or vacancies in the intergranular zones, which generate new energy levels and, as a result, diminish the band gap energy [22, 23].

Table 4 – Summarize of morphological, structural and optical parameters of undoped and doped NiO nanostructured films.

Samples	D_{111}	D_{200}	E_g	E_u	t : thickness	Ra : roughness
	(nm)	(nm)	(eV)	(meV)	(nm)	(nm)
Undoped NiO	11.95	14.85	3.742	262.977	360.3	23.26
Ba 2 at.% NiO	16.80	13.70	3.693	356.642	213.2	27.89
Ba 4 at.% NiO	19.20	19.58	3.644	334.164	240.5	30.35
Ba 6 at.% NiO	9.59	8.54	3.638	327.337	375.6	36.46
Ba 8 at.% NiO	33.02	53.53	3.503	303.144	236.5	39.06

They are, however, greater than the value (3.51 eV) reported for NiO nanopowder made by the sol-gel process and calcined at 400 °C for 3 hours [24], as well as the value (3.55 eV) published by Boschloo and Hagfeldt [25].

The estimation procedure of the optical band gap of undoped NiO and Ba doped NiO thin films formed at 450 °C is shown in Fig. 5a-e.

Fig. 8, illustrates what is known as localized states, which appear in band tails at the boundaries of the band gap, the valence and conduction bands. The extended states are found for energies higher than E_c and less than E_v (Fig. 7 and Table 4); this difference is known as the energy of disorder. When the disorder gets too high (for example, when hanging bonds or impurities occur in the material), the tails may become entangled. The meaning of Urbach parameter (E_u) will then be defined, which relates to transitions between the extended states of the valence band and the localized states of the conduction band.

As mentioned by [17], we determined the Urbach tail energy (E_u) from the absorption coefficient which is exponentially related to the disorder according to the following law:

$$A = A_0 \cdot \exp\left(\frac{hv}{E_u}\right), \quad (7)$$

Where A_0 is a constant, hv denotes photon energy, and E_u denotes Urbach energy.

Fig. 6f depicts the method for estimating the Urbach energy of undoped NiO and Ba doped NiO thin films formed at 450 °C (Table 4).

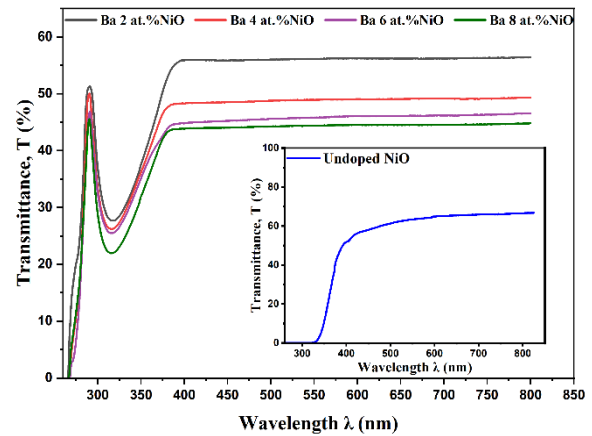


Fig. 5 – Transmittance curves vs wavelength of undoped sample (inset) and Ba-doped (0, 2, 4, 6 and 8 at. %) NiO thin films prepared at 450 °C

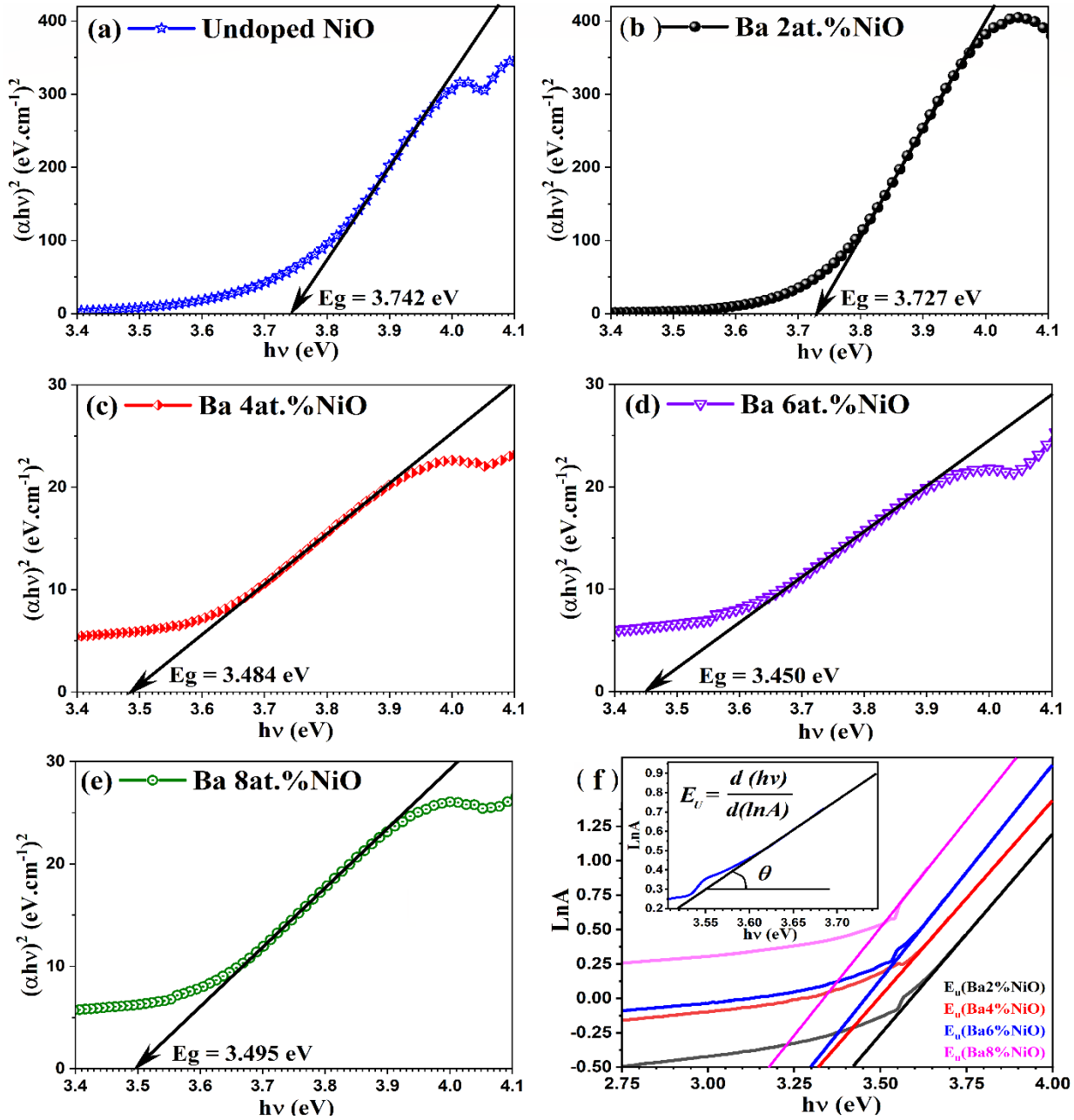


Fig. 6 – Plots of $(\alpha hv)^2$ vs $h\nu$ for: (a) undoped NiO, (b) Ba 2 at. % NiO, (c) Ba 4 at. % NiO, (d) Ba 6 at. % NiO, (e) Ba 8 at. % NiO and (f) Plots of $\ln(\alpha)$ vs $h\nu$ for all Ba doped NiO thin films

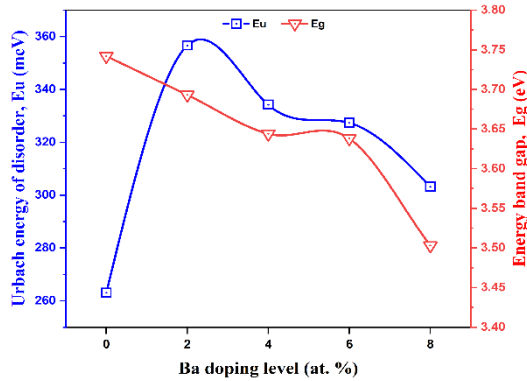


Fig. 7 – Variation of the optical band gap energy and Urbach energy of undoped NiO and Ba doped NiO thin films

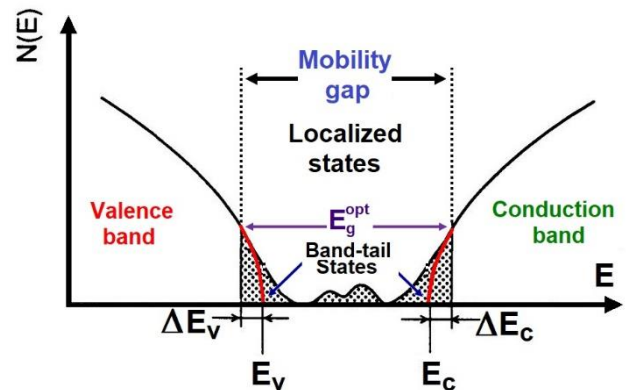


Fig. 8 – Variation of the optical band gap energy and Urbach energy of undoped NiO and Ba doped NiO thin films

4. CONCLUSIONS

In summary, the influence of the percentage of the doping element Ba on structural, morphological and optical characteristics of NiO thin films of NiO was investigated in this work. Pure and Ba-doped NiO thin films were successfully prepared by pneumatic spray pyrolysis method on glass substrates heated at 450 °C. The XRD patterns of the samples show a face-centered cubic structure corresponding to the NiO structure with polycrystalline phases. The whole obtained films have a nanocrystalline cubic structure and are mainly (111) oriented.

We observed an improvement in the crystallinity of the thin layers deposited as the percentage of the barium-doped solution increased from 2 at. % to 8 at. %. The crystallites increase in size but remain in the nanometric range. The optical band gap decreased from 3.742 to

3.503 eV as Ba concentration increased. The Urbach energy of disorder varies between 262.977 and 356.642 meV. The morphology of the films evaluated by SEM reveals a rough and textured surface with varying degrees of roughness depending on the level of Ba-doping: roughness increased as Ba concentration increased.

ACKNOWLEDGEMENTS

The authors would like to express their gratitude to Professor N. Dizge of the University of Mersin (Turkey) for his warm welcome and assistance with the SEM study. The authors would like to thank the staff of the Ouargla physical-chemical analysis technological platform (PTAPC) for their support in performing the UV-visible spectrometric analysis.

REFERENCES

1. K. Bädeker, *Ann. Phys.* **327**, 749 (1907).
2. J.T. Littleton. Pat. US 2,118,795 USA, publi. 1938-05-24.
3. J.M. Mochel. Pat. US 2,564,706 A, USA, publi. 1951-08-21.
4. Harold A. McMaster. Pat. US 2,429,420 A, USA, publi. 1947-10-21.
5. W.O. Lytle, A.E. Junge. Pat. US 2,566,346 A, USA, publi. 1951-09-04.
6. M.J. Zunick. Pat. US 2,516,663 A, USA, publi. 1950-07-25.
7. J.M. Mochel. Pat. US 2,564,707 A, USA, publi. 1951-08-2.
8. E. Scharowsky, *Z. Phys.* **135**, 318 (1953).
9. K. Wasa, S. Hayakawa, T. Hada, *Jpn. J. Appl. Phys.* **10**, 1732 (1971).
10. A. Charef, S. Benramache, Y. Aoun, B. Benhaoua, S. Lakel, M. Marrakchi, *J. Nanoelectron. Optoelectron.* **14**, 1667 (2019).
11. T. Çayır Taşdemirci, *Vacuum* **167**, 189 (2019).
12. S. Boulila, M. Ghamnia, A. Boukhachem, A. Ouhaibi, M.A. Chakhoun, C. Fauquet, V. Heresanu, D. Tonneau, *Philos. Mag. Lett.* **100**, 283 (2020).
13. A.D. Cullity, S.R. Stock, *Elements of X-ray Diffraction* (New York- Prentice-Hall: 2001).
14. S. Muthukumaran, R. Gopalakrishnan, *Opt. Mater.* **34**, 1946 (2012).
15. S. Benramache, B. Benhaoua, *Superlattice. Microstruct.* **52**, 807 (2012).
16. N.A. Hameed, I.M. Ali, H.K. Hassun, *Energy Procedia*, **157**, 84 (2019).
17. S. Benramache, Y. Aoun, S. Lakel, H. Mourghade, R. Gacem, B. Benhaoua, *J. Nano- Electron. Phys.* **10**, 06032 (2018).
18. W.J. Leng, C.R. Yang, H. Ji, J.H. Zhang, H.W. Chen, J.L. Tang, *J. Appl. Phys.* **100**, 083505 (2006).
19. C. Aydın, S.A. Mansour, Z.A. Alahmed, F. Yakuphanoglu, *J. Sol-Gel Sci. Technol.* **62**, 397 (2012).
20. J.G. Marek Guziewicz, M. Borysiewicz, E. Kaminska, J. Z. Domagala, W. Rzdokiewicz, B.S. Witkowski, K. Golaszewska, R. Kruszka, M. Ekielski, A. Piotrowska, *Opt. Appl.* **41**, 431 (2011).
21. A.J. Varkey, A.F. Fort, *Thin Solid Films* **235**, 47 (1993).
22. L. Soriano, M. Abbate, J. Vogel, J.C. Fuggle, A. Fernández, A.R. González-Elipe, M. Sacchi, J.M. Sanz, *Chem. Phys. Lett.* **208**, 460 (1993).
23. H. Yamamoto, S. Tanaka, K. Hirao, *J. Appl. Phys.* **93**, 4158 (2003).
24. M. Alagiri, S. Ponnusamy, C. Muthamizchelvan, *J. Mater. Sci.: Mater. Electron.* **23**, 728 (2012).
25. G. Boschloo, A. Hagfeldt, *J. Phys. Chem. B* **105**, 3039 (2001).

Морфологічні, структурні та оптичні властивості наноструктурних тонких плівок NiO, легованих Ba

M.Z. Merad¹, L. Fellah², A. Diha³

¹ *Exploitation et Valorisation des Ressources Naturelles en Zones Arides, 30000 Ouargla, Algeria*

² *Faculty of Hydrocarbons and Renewable Energies and Earth and Universe Sciences, University of Kasdi Merbah, 30000 Ouargla, Algeria*

³ *Department of Mechanical Engineering, University Larbi Tébessi, Tébessa 12000, Algeria*

У статті повідомляється про вплив легування барієм на властивості тонких плівок NiO. Нелеговані та леговані плівки були нанесені на скляну підкладку при 450 °C за допомогою техніки пневматичного розпилювального піролізу (PSPT) з різними концентраціями барію (0 – 8 ат.%). Рентгенівські дифракційні картини показують полікристалічну природу плівок із переважною орієнтацією (111). Жодних інших кластерів і домішкових фаз металевого барію не спостерігалось при легуванні Ba. Розмір кристалів осаджених тонких плівок розраховували за формулою Дебая-Шеррера для двох орієнтацій (111) і (200), і на фотографіях SEM ми знайшли значення в діапазоні від 11,95 до 39,06 нм в обох випадках. У видимій області оптичне пропускання тонких плівок NiO, легованих Ba, впало на 46 % порівняно з нелегованими тонкими плівками NiO (79 %). Було виявлено, що ширина забороненої зони зменшується в діапазоні 3,742 – 3,503 eV з легуванням Ba. Енергія безладу Урбаха явно зростає від 262,98 до 356,64 меВ при переході від нелегованого тонкого шару до тонкого шару, легованого при 2 ат. %, потім зменшується до мінімуму 303,14 меВ для легування барієм 8 ат. %, дозволяючи атомам знайти хороше місце, тобто тонкі плівки стають однорідними та сильно кристалізованими. Шорсткість була розрахована за допомогою аналізу SEM зображень. Її значення коливалися в межах 23,26 – 39,06 нм.

Ключові слова: Розпилювальний піроліз, NiO Легований Ba, Тонкі плівки, Заборонена зона, Енергія Урбаха, Розмір зерна.